Electronic Supplementary Material (ESI) for Inorganic Chemistry Frontiers.

Orange to Red Iridium(III) Complexes Possessing Good Electron Mobility with pyrimidine-4-carboxylic acid ligand for High-Performance Solution-Processed OLEDs with an EQE over 31%

Tao Han [a, #], Yan Xia [b, #], Xin-yu Zhang [a], Yu-qiao Tong [a], Ming-yu Teng [a, *], Chong-yang Shi [a, *], Long-wu Ye [a], Zhao Chen [b, *], Shuo-qi Sun [c], and Guangzhao Lu [d, *]

[a] Faculty of Chemistry and Chemical Engineering, Yunnan Normal University, Kunming 650500, PR China.

[b] School of Applied Physics and Materials, Wuyi University, Jiangmen, 529020, P. R. China

[c] Hongzhiwei Technology (Shanghai) Co. Ltd., 1599 Xinjinqiao Road, Pudong, Shanghai 200137, PR China.

[d] Shenzhen Institute of Information Technology, Shenzhen 518172, PR China.

[#] These authors contributed equally to this work.

Corresponding Authors

Mingyu Teng, Email: myteng@ynnu.edu.cn

Zhao Chen, Email: chenzhao2006@163.com

Guangzhao Lu, Email: lugz@sziit.edu.cn

Table of Contents

Materials and Measurements

All reagents and chemicals were purchased from commercial sources and used without further purification. ^{1}H and ^{13}C nuclear magnetic resonance (NMR) spectra were recorded using a Bruker spectrometer at 500 MHz using TMS as an internal standard. High-resolution mass spectra (HRMS) were measured by Thermo Scientific Q Exactive mass spectrometer. Thermo gravimetric analyses (TGAs) were performed on a TA Discovery SDT 650 instrument under nitrogen with a heating rate of 10 °C min^{-1}. The absorption and photoluminescence spectra were measured on a Shimadzu UV-2700 recording spectrophotometer and a Hitachi F-7100 photoluminescence spectrophotometer. The luminescence quantum efficiencies were calculated by comparison of the emission intensities of a standard sample (fac-$Ir(ppy)_3$) and the unknown sample.

Synthesis of Ligands and Iridium Complexes

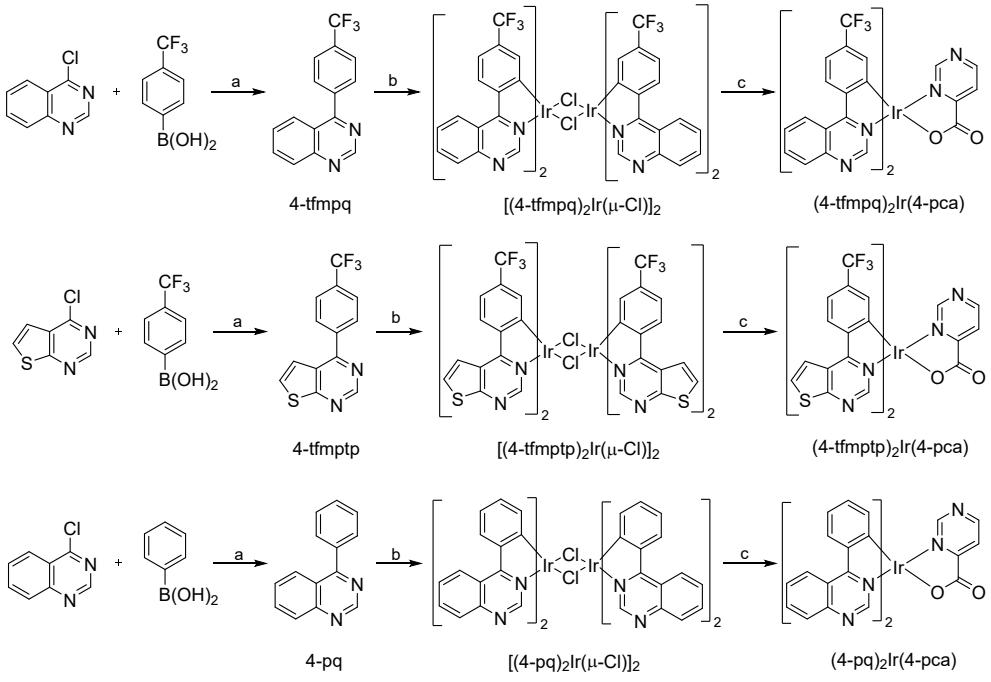

Scheme S1 The synthetic routes of the ligands and Ir(III) complexes: (a) $Pd(PPh_3)_4$, Na_2CO_3, THF-H_2O, 80 °C, 12 h; (b) $IrCl_3$, $EtOCH_2CH_2OH$-H_2O, 110 °C, 12 h; (c) 4-pca, $EtOCH_2CH_2OH$, 110 °C, 24 h.

The main ligands 4-(4-(trifluoromethyl)phenyl)quinazoline (4-tfmpq), 4-(4-(trifluoromethyl)phenyl)thieno[2,3-d]pyrimidine (4-tfmptp), 4-phenylquinazoline (4-pq) were synthesized according to the reported procedure. 4-tfmpq.[1] Yield: 82%. ^{1}H NMR (500 MHz, $CDCl_3$) δ 9.44 (s, 1H), 8.19 (d, *J* = 8.5 Hz, 1H), 8.08 (d, *J* = 8.4 Hz, 1H), 7.99 (t, *J* = 7.7 Hz, 1H), 7.94 (d, *J* = 8.1 Hz, 2H), 7.88 (d, *J* = 8.2 Hz, 2H), 7.68 (t, *J* = 7.7 Hz, 1H). 4-tfmptp. Yield: 92%. ^{1}H NMR (500 MHz, $CDCl_3$) δ 9.22 (s, 1H), 8.10 (d, *J* = 8.0 Hz, 2H), 7.86 (d, *J* = 8.1 Hz, 2H), 7.67 (d, *J* = 6.1 Hz, 1H), 7.59 (d, *J* = 6.1 Hz, 1H). 4-pq. Yield: 66%. ^{1}H NMR (500 MHz, $CDCl_3$) δ 9.41 (s, 1H), 8.17 – 8.12 (m, 2H), 7.94 (ddd, *J* = 8.3, 6.9, 1.4 Hz, 1H), 7.83 – 7.78 (m, 2H), 7.63 (ddd, *J* = 8.3, 5.6, 1.3 Hz, 1H), 7.61 – 7.58 (m, 3H).

The $IrCl_3 \cdot 3H_2O$ (0.76 g, 2.14 mmol) and 2.5 equivalent of cyclometalated ligand (5.35 mmol) were added in a 2-ethoxyethanol and water mixture. Then, the solution was heated for 12 h at 110 °C. After the addition of water, precipitated powder of $[(C\hat{}N)_2Ir(\mu\text{-}Cl)]_2$ chloride-bridged dimer was filtered and reacted with 4-pac for 24 h at 110 °C. The solution was concentrated, and the resulting residue was purified by silica gel column chromatography (CH_2Cl_2/methanol 15:1 (v/v)).

$(4\text{-tfmpq})_2Ir(4\text{-pca})$: Yield: 55%. ^{1}H NMR (500 MHz, $CDCl_3$) δ 9.44 (s, 1H), 8.99 (d, J = 4.9 Hz, 1H), 8.88 (t, J = 8.5 Hz, 2H), 8.56 (d, J = 8.4 Hz, 1H), 8.46 (d, J = 8.4 Hz, 1H), 8.36 (s, 2H), 8.24 (t, J = 6.0 Hz, 3H), 8.16 (d, J = 8.4 Hz, 1H), 8.02 (t, J = 7.7 Hz,

3H), 7.90 (dt, J = 7.0, 6.4 Hz, 3H), 7.39 (d, J = 7.9 Hz, 1H), 7.30 (d, J = 8.2 Hz, 1H), 6.88 (s, 1H), 6.46 (s, 1H). ^{13}C NMR (126 MHz, $CDCl_3$) δ 174.79 (s), 173.41 (s), 170.44 (s), 159.80 (s), 157.89 (s), 157.72 (s), 153.48 (s), 152.45 (s), 151.98 (s), 151.51 (s), 151.40 (s), 151.12 (s), 147.29 (s), 147.10 (s), 135.68 (s), 132.42 (s), 132.05 (s), 129.82 (s), 129.71 (d, J = 3.9 Hz), 129.33 (s), 129.17 (s), 126.12 (s), 125.34 (s), 123.58 (s), 121.96 (s), 121.54 (s), 119.57 (s), 119.11 (s). HR-MS calcd for $C35H19F6IrN6O2^+$ $[M+H]^+$ 863.1181, found 863.1169.

$(4\text{-tfmptp})_2$Ir(4-pca): Yield: 18%. ^{1}H NMR (500 MHz, $CDCl_3$) δ 9.31 (s, 1H), 9.04 (d, J = 4.9 Hz, 1H), 8.43 (s, 1H), 8.41 (d, J = 8.4 Hz, 1H), 8.35 (d, J = 8.4 Hz, 1H), 8.27 (d, J = 4.9 Hz, 1H), 8.23 (s, 1H), 8.21 (d, J = 6.2 Hz, 2H), 7.95 (t, J = 6.3 Hz, 2H), 7.40 (d, J = 8.4 Hz, 1H), 7.32 (d, J = 8.3 Hz, 1H), 6.83 (s, 1H), 6.43 (s, 1H). ^{13}C NMR (126 MHz, $CDCl_3$) δ 171.16 (s), 170.83 (s), 170.49 (s), 168.65 (s), 167.47 (s), 159.82 (s), 157.73 (s), 152.30 (s), 151.61 (s), 151.10 (s), 150.60 (s), 131.40 (s), 131.07 (s), 129.86 (s), 129.39 (s), 128.95 (s), 126.22 (s), 125.61 (s), 123.66 (s), 120.00 (s), 119.77 (s), 119.41 (s). HR-MS calcd for $C31H15F6IrN6O2S2^+$ $[M+H]^+$ 875.0310, found 875.0302.

$(4\text{-pq})_2$Ir(4-pca): Yield: 51%. ^{1}H NMR (500 MHz, $CDCl_3$) δ 9.40 (s, 1H), 8.95 (d, J = 4.9 Hz, 1H), 8.89 (t, J = 7.4 Hz, 2H), 8.43 (d, J = 8.1 Hz, 1H), 8.35 (d, J = 5.3 Hz, 2H), 8.30 (s, 1H), 8.22 (d, J = 4.5 Hz, 1H), 8.18 (d, J = 8.4 Hz, 1H), 8.09 (d, J = 8.3 Hz, 1H), 7.94 (t, J = 7.3 Hz, 2H), 7.82 (dd, J = 14.5, 7.1 Hz, 2H), 7.12 (t, J = 7.5 Hz, 1H), 7.03 (t, J = 7.5 Hz, 1H), 6.91 (t, J = 7.4 Hz, 1H), 6.83 (t, J = 7.3 Hz, 1H), 6.71 (d, J = 7.7 Hz, 1H), 6.33 (d, J = 7.7 Hz, 1H). ^{13}C NMR (126 MHz, $CDCl_3$) δ 176.14 (s), 174.71 (s),

170.56 (s), 159.19 (s), 158.10 (s), 158.04 (s), 155.18 (s), 153.67 (s), 152.51 (s), 151.93 (s), 151.11 (s), 150.79 (s), 143.76 (s), 143.48 (s), 134.92 (s), 134.06 (s), 133.54 (s), 132.62 (d, J = 5.5 Hz), 132.42 (s), 132.05 (s), 129.44 (s), 128.86 (d, J = 13.9 Hz), 126.63 (s), 125.90 (s), 123.34 (s), 122.45 (s), 122.04 (s), 121.81 (s), 121.46 (s). HR-MS calcd for $C_{33}H_{21}IrN_6O_2^+$ $[M+H]^+$ 727.1433, found 727.1432.

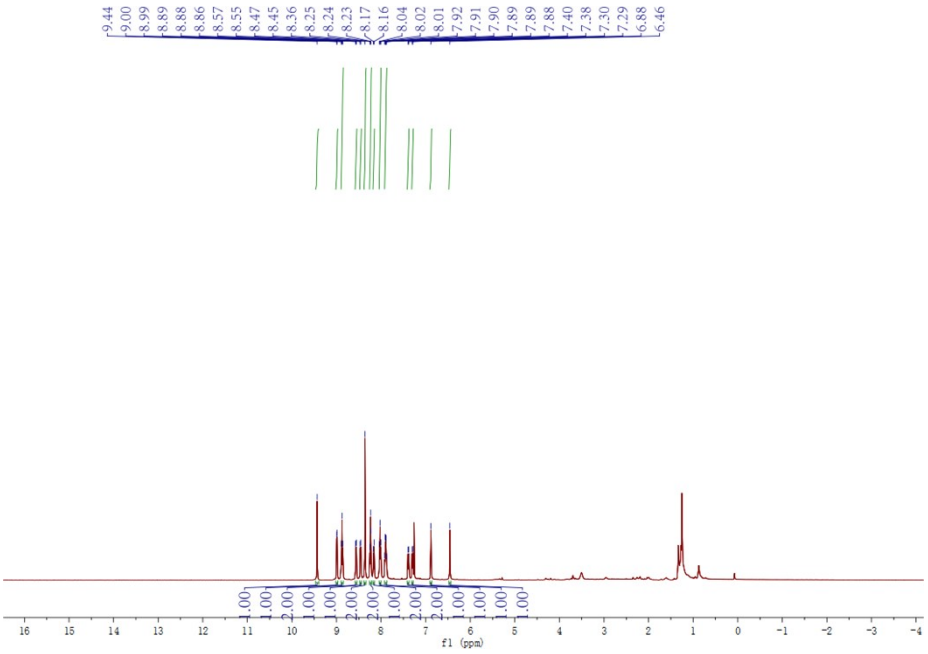

Fig. S1 ^{1}H NMR spectrum of $(4\text{-tfmpq})_2\text{Ir}(4\text{-pca})$.

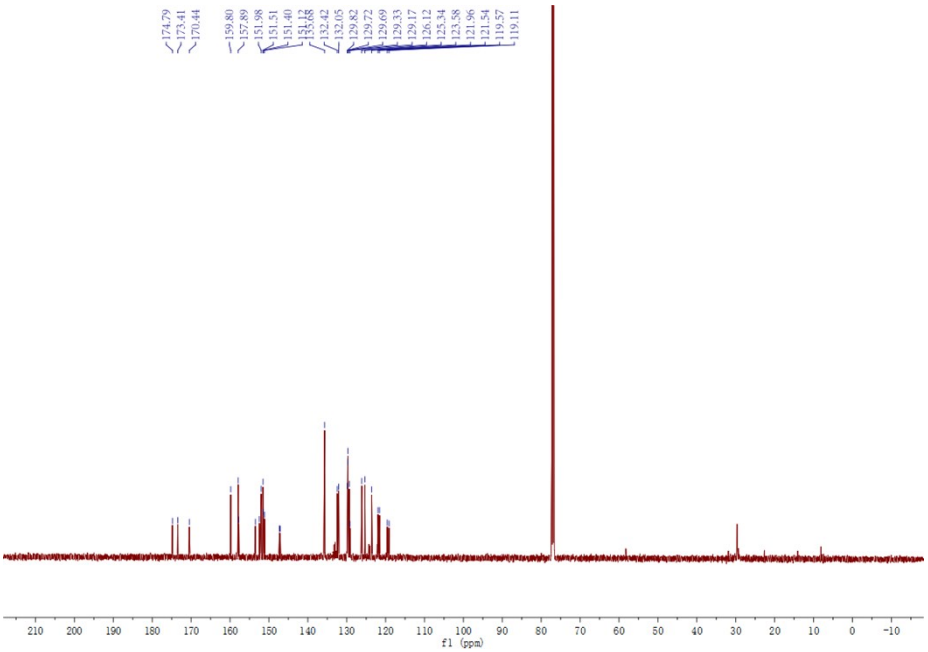

Fig. S2 ^{13}C NMR spectrum of (4-tfmpq)$_2$Ir(4-pca).

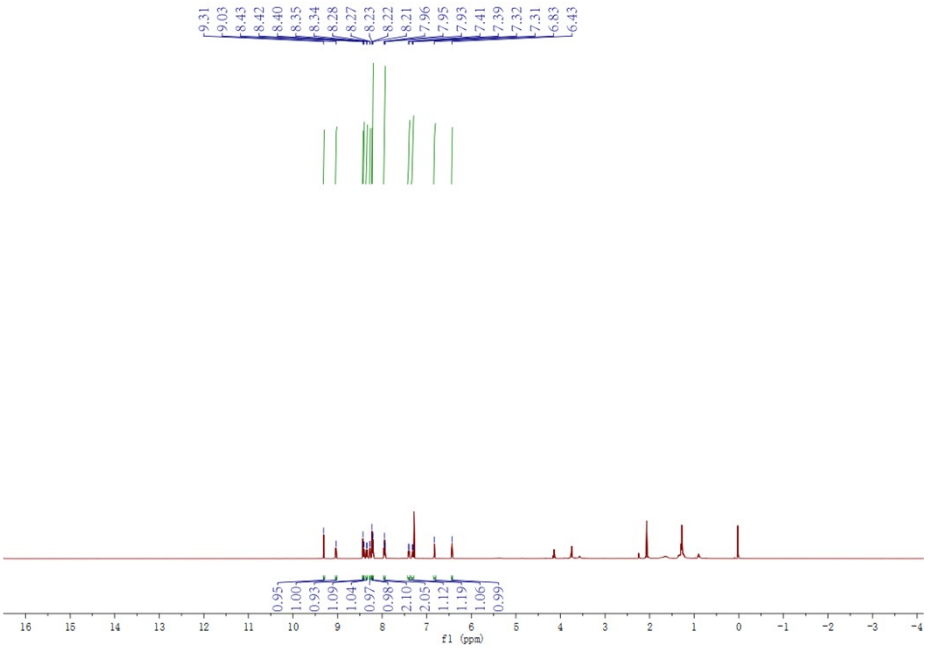

Fig. S3 ^{1}H NMR spectrum of (4-tfmptp)$_2$Ir(4-pca).

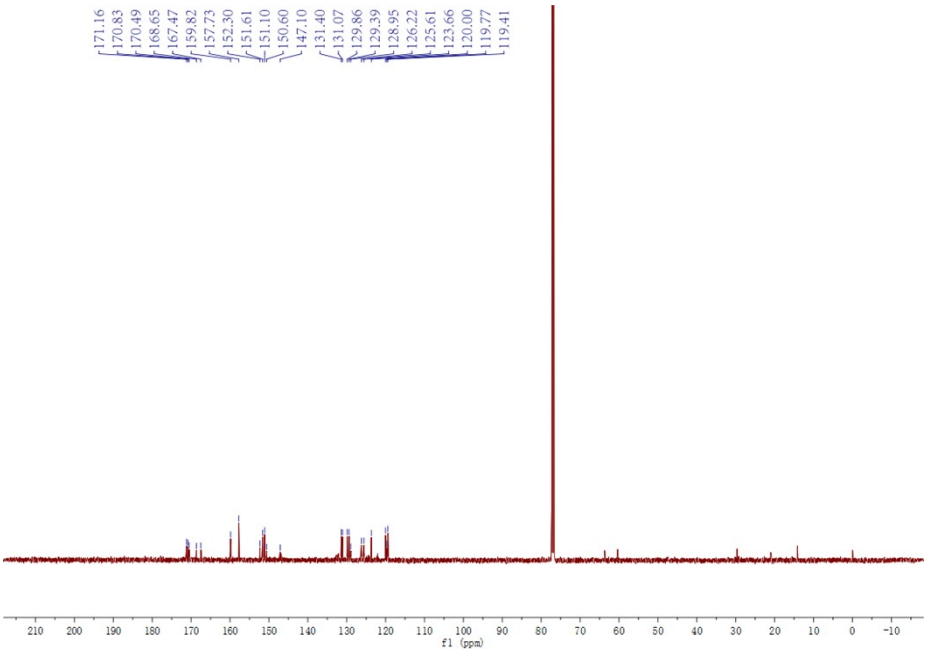

Fig. S4 ^{13}C NMR spectrum of (4-tfmptp)$_2$Ir(4-pca).

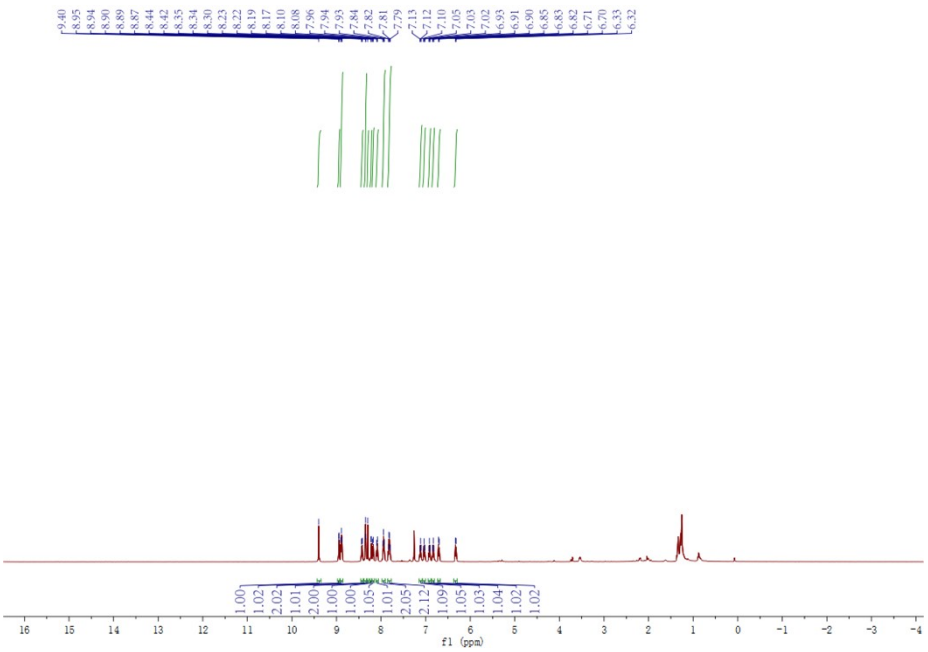

Fig. S5 ^{1}H NMR spectrum of (4-pq)$_2$Ir(4-pca).

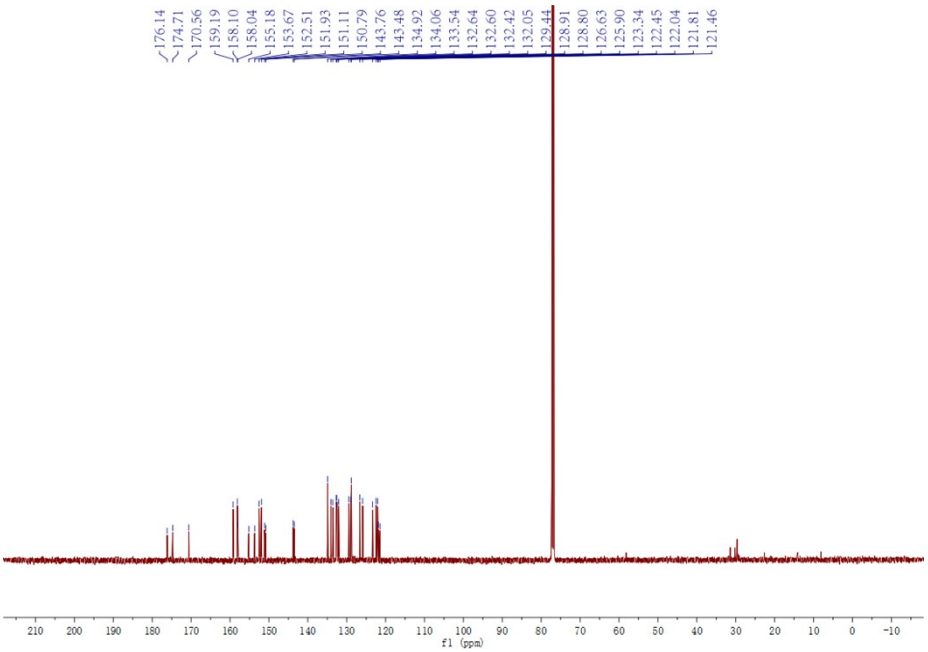

Fig. S6 ^{13}C NMR spectrum of $(4\text{-pq})_2Ir(4\text{-pca})$.

X-ray Crystallography

The single crystals of the three complexes were obtained from the slow evaporation of methanol /CH_2Cl_2 solution at room temperature. Its X-ray-diffraction data were carried out on a D8 venture diffractometer using monochromated Mo Kα radiation (λ= 0.71073 Å) at 100K. Cell parameters were retrieved using SMART software and refined using SAINT on all observed reflections. Data were collected using a narrow-frame method with scan widths of 0.30° in ω and an exposure time of 10 s/frame. Crystal structures were solved by direct methods using the SHELXL-2014/7' software. None-hydrogen atoms were refined anisotropically by full-matrix least-squares calculations on F^2 using SHELXL-2014/7', while the hydrogen atoms were introduced at the calculated position and refined in the riding mode.

Cyclic Voltammetry Measurements and Theoretical Calculations

Cyclic voltammetry (CV) was measured on a CHI voltammetric analyzer at room temperature with the conventional three-electrode configuration, consisting of a platinum column working electrode, a platinum wire auxiliary electrode, and an Ag wire pseudo reference electrode. Cyclic voltammograms were recorded using tetrabutylammonium hexafluorophosphate ($TBAPF_6$) (0.1 M) dissolved in dichloromethane (5 mL) as the supporting electrolyte, and ferrocenium-ferrocene (Fc^+/Fc) as the external standard, at the scan rate of 100 mV s^{-1}. The onset potential was determined from the intersection of two tangents of the rising and background current in a cyclic voltammogram. We perform theoretical calculations employing Device Studio software with B3LYP function. The basis set of 6-31G (d, p) was used for C, H, N, S, O, and F atoms, while the LanL2DZ basis set was employed for Ir atoms.

OLEDs Fabrication and Measurement

All the devices were grown on glass substrates pre-coated with a 160 nm-180 nm thick layer of indium tin oxide (ITO) with a sheet resistance of 10 Ω per square. Before loading into the deposition system, the ITO substrates were pre-cleaned carefully, and the surface was treated with oxygen plasma for 15 minutes. After UV ozone treatment, PEDOT:PSS(35nm)/PVK(5nm)/(CBP: Ir 1wt%)were sequentially spin-coated on the ITO. Finally, TmPyPB(40nm) and a cathode composed of lithium fluoride (LiF, 1nm)/aluminum (Al, 120 nm) was sequentially deposited onto the substrate in a vacuum of 10^{-6} Pa. The current density-voltage-luminance (J-V-L) characteristics were

measured using a Keithey 2400 Source meter and a Keithey 2000 Source multimeter equipped with a calibrated silicon photodiode. The EL spectra were tested using a brightness light distribution characteristics measurement system C9920-11. The EQE of the EL device was calculated based on the photo energy examined using the photodiode, the EL spectrum and the current passing through the device. All measurements were carried out at room temperature under ambient conditions.

Tables and Figures

Table S1 The crystallographic data of (4-tfmpq)$_2$Ir(4-pca), (4-tfmptp)$_2$Ir(4-pca) and (4-pq)$_2$Ir(4-pca).

	(4-tfmpq)$_2$Ir(4-pca)	**(4-tfmptp)$_2$Ir(4-pca)**	**(4-pq)$_2$Ir(4-pca)**
Empirical formula	$C_{35}H_{19}F_6IrN_6O_2$	$C_{31}H_{15}F_6IrN_6O_2S_2$	$C_{33}H_{21}IrN_6O_2$
Formula weight	861.76	873.81	725.76
T / K	100	100	100
Wavelength (Å)	0.71073	0.71073	0.71073
Crystal system	monoclinic	orthorhombic	monoclinic
Space group	$C2/c$ (15)	$Pbca$ (61)	$I2/a$ (15)
a / Å	23.8664(14)	10.0618(6)	17.1167(11)
b / Å	15.4400(8)	20.7300(13)	17.0189(5)
c / Å	17.1443(8)	26.6333(17)	18.3944(7)
α (deg)	90	90	90
β (deg)	101.336(2)	90	104.640(4)
γ (deg)	90	90	90
V / Å3	6194.4(6)	5555.2(6)	5184.5(4)
Z	8	8	8
ρcalcd / g cm-3	1.848	2.090	1.860

μ / mm-1	4.392	5.043	5.196
F(000)	3344	3376	2832
GOF on F^2	1.027	1.106	1.070
Reflns collected	57126	5905	31182
Unique(Rint)	7701（0.0515）	5905（0.068）	6465（0.0661）
R_1, wR_2 [I > 2σ(I)]a	0.0219, 0.0487	0.0571,0.0957	0.0383,0.0793
R1, wR2 (all data)	0.0298, 0.0516	0.0846,0.1032	0.0751, 0.0922

$R_1{}^a = \Sigma||F_o| - |F_c||/ \Sigma F_o|$. $wR_2{}^b = [\Sigma w(F_o{}^2 - F_c{}^2)^2/ \Sigma w(F_o{}^2)]^{1/2}$

Table S2 Selected bond lengths (Å) of $(4\text{-tfmpq})_2$Ir(4-pca), $(4\text{-tfmptp})_2$Ir(4-pca) and $(4\text{-pq})_2$Ir(4-pca).

		$(4\text{-tfmpq})_2$Ir(4-pca)			
Ir–O(1)	2.1513(18)	Ir–N(1)	2.039(2)	Ir–N(3)	2.133(2)
Ir–N(5)	2.045(2)	Ir–C(21)	1.989(3)	Ir–C(14)	1.996(3)
		$(4\text{-tfmptp})_2$Ir(4-pca)			
Ir–O(1)	2.156(5)	Ir–N(1)	2.039(6)	Ir–N(3)	2.056(6)
Ir–N(5)	2.142(6)	Ir–C(6)	2.018(3)	Ir–C(17)	2.030(3)
		$(4\text{-pq})_2$Ir(4-pca).			
Ir–O(1)	2.171(4)	Ir–N(1)	2.029(5)	Ir–N(3)	2.148(5)
Ir–C(5)	1.987(6)	Ir–N(5)	2.048(5)	Ir–C(16)	1.997(6)

Table S3 Selected angles (°) of $(4\text{-tfmpq})_2$Ir(4-pca), $(4\text{-tfmptp})_2$Ir(4-pca) and $(4\text{-pq})_2$Ir(4-pca)

		$(4\text{-tfmpq})_2$Ir(4-pca)			
N(1)–Ir–O(1)	87.25(8)	N(5)–Ir–O(1)	97.29(8)	C(21)–Ir–N(3)	97.28(9)
N(1)–Ir–N(3)	98.61(8)	N(5)–Ir–N(3)	91.37(8)	C(21)–Ir–N(5)	79.73(10)
N(1)–Ir–N(5)	169.77(9)	C(21)–Ir–O(1)	173.35(8)	C(21)–Ir–C(14)	90.61(10)
N(3)–Ir–O(1)	76.77(8)	C(21)–Ir–N(1)	96.67(9)	C(14)–Ir–O(1)	95.40(9)
C(14)–Ir–N(1)	79.46(10)	C(8)–N(1)–Ir	117.57(18)	C(20)–N(3)–Ir	127.33(18)

C(14)–Ir–N(3)	172.06(9)	C(8)–N(1)–C(1)	119.2(2)	C(20)–N(3)–C(17)	117.9(2)
C(14)–Ir–N(5)	90.96(10)	C(1)–N(1)–Ir	123.17(17)	C(27)–N(5)–Ir	115.28(17)
C(16)–O(1)–Ir	116.99(16)	C(17)–N(3)–Ir	114.54(17)	C(27)–N(5)–C(30)	119.2(2)
		$(4\text{-tfmptp})_2$Ir(4-pca)			
N(1)–Ir–O(1)	94.4(2)	N(1)–Ir–N(3)	176.4(2)	N(1)–Ir–N(5)	89.0(2)
N(3)–Ir–O(1)	85.5(2)	N(3)–Ir–N(5)	94.5(2)	N(5)–Ir–O(1)	77.0(2)
C(6)–Ir–O(1)	172.56(19)	C(6)–Ir–N(1)	79.6(2)	C(6)–Ir–N(3)	100.7(2)
C(6)–Ir–N(5)	98.2(2)	C(17)–Ir–N(3)	79.7(2)	C(17)–Ir–O(1)	96.6(2)
C(17)–Ir–N(1)	96.7(2)	C(21)–N(3)–Ir	115.5(5)	C(17)–Ir–N(5)	171.8(2)
C(27)–O(1)–Ir	115.5(5)	C(26)–N(3)–Ir	124.7(5)	F(1)–C(1)–F(3)	106.4(7)
C(8)–N1–Ir	117.4(5)	C(13)–N(1)–Ir	121.9(5)		
		$(4\text{-pq})_2$Ir(4-pca)			
N(1)–Ir–O(1)	93.95(17)	C(5)–Ir–N(3)	171.5(2)	C(6)–N(1)–Ir	121.4(4)
N(1)–Ir–N(3)	93.37(19)	C(5)–Ir–N(5)	79.6(2)	C(24)–N(1)–Ir	118.5(4)
N(1)–Ir–N(5)	172.25(19)	C(5)–Ir–C(16)	88.1(2)	C(24)–N(1)–C(6)	119.8(5)
N(3)–Ir–O(1)	76.24(18)	C(16)–Ir–O(1)	171.60(19)	C(6)–N(2)–C(13)	116.0(5)
N(5)–Ir–O(1)	84.70(17)	C(16)–Ir–N(1)	79.7(2)	C(21)–N(3)–Ir	114.6(4)
N(5)–Ir–N(3)	93.71(19)	C(16)–Ir–N(3)	98.5(2)	C(21)–N(3)–C(31)	117.9(5)
C(5)–Ir–O(1)	97.73(19)	C(16)–Ir–N(5)	102.3(2)	C(31)–N(3)–Ir	127.2(4)
C(5)–Ir–N(1)	93.0(2)	C(1)–O(1)–Ir	117.1(4)	C(15)–N(4)–C(31)	115.8(6)

Table S4 The electronic cloud density distributions of three complexes.

Complex	Orbital	Energy/eV	Energy/eV	Composition (%)		
		(Calculated)	(Experimental)	Main ligand	Ir	Ancillary Ligand
$(4\text{-tfmpq})_2$Ir(4-pca)	HOMO	-5.72	-5.85	51.57	41.19	7.24
	LUMO	-2.67	-3.75	93.18	4.39	2.43
$(4\text{-tfmptp})_2$Ir(4-pca)	HOMO	-5.73	-5.85	43.77	48.72	7.51
	LUMO	-2.52	-3.54	93.44	2.50	4.06
$(4\text{-pq})_2$Ir(4-pca)	HOMO	-5.35	-5.60	44.36	48.14	7.49
	LUMO	-2.34	-3.57	92.67	4.35	2.98

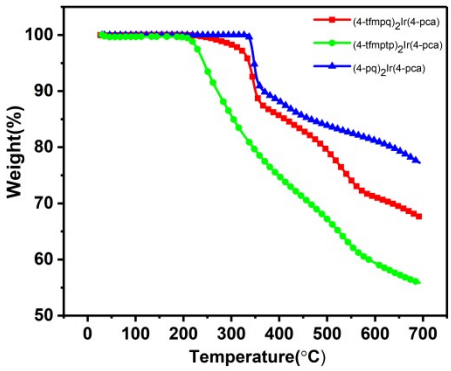

Fig. S7 The TG curves of the three complexes.

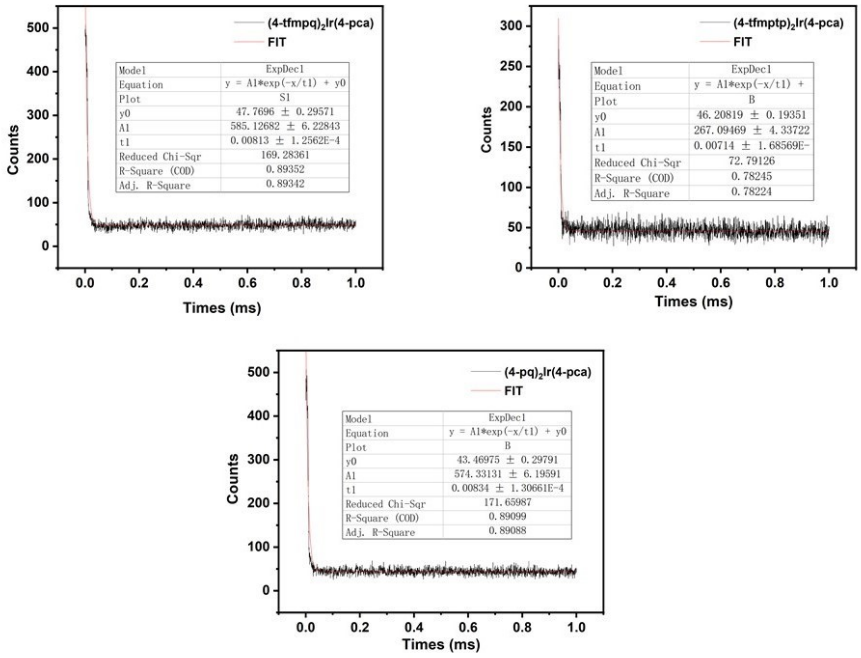

Fig. S8 The lifetime curves of the (4-tfmpq)$_2$Ir(4-pca), (4-tfmptp)$_2$Ir(4-pca) and (4-pq)$_2$Ir(4-pca) complexes in degassed dichloromethane solutions (10^{-5} M).

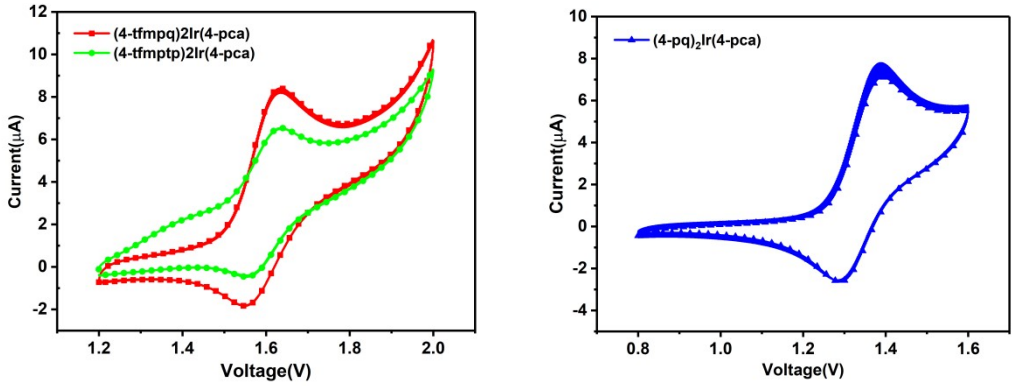

Fig. S9 Cyclic voltammograms of the iridium (III) complexes and Fc/Fc^{+}.

Table S5 The reported solution-processed OLEDs employing Ir complexes with emission at 510-630 nm.

Name	CIE (x,y)	$\eta_{c,max}$ (cd A^{-1})	$\eta_{ext,max}$ (%)	Reference
$Ir(tpp)_2(paz)$	(0.37, 0.60)	41.7	10.5	Inorganica Chimica Acta. 516 (2021) 120100.
$(Dfppy)_4Ir_2(ecbtpd)$	(0.40,0.53)	23.67	8.44	J. Organomet. Chem. 1001 (2023) 122850.
$Ir(ppm)_2(taz)$	(0.35,0.60)	40.4	17.3	RSC Adv. 6 (2016) 34970-34976.
$Ir(tpp)_2(paz)$	(0.37, 0.60)	41.7	10.5	Inorganica Chimica Acta. 516 (2021) 120100.
Ir-3Tz2F	(0.31,0.58)	26.7	8.0	J. Mater. Chem. C. 5 (2017) 208-219.
$[Ir(mpmi)_2(imp)]PF_6$	(0.51, 0.47)	6.36	2.8	Dyes. Pigments. 134 (2016) 465-471.
$[Ir(mpmi)_2(pymbi)]PF_6$	(0.47, 0.51)	17.42	6.4	Dyes. Pigments. 134 (2016) 465-471.
$Ir(ppm)_2(pic)$	(0.40,0.50)	30.6	10.4	RSC Adv. 6 (2016) 34970-34976.
Ir-3Tz1F	(0.37,0.59)	56.2	15.8	J. Mater. Chem. C. 5 (2017) 208-219.
$Ir(2\text{-}Flfupy)_3$	(0.54, 0.45)	34.2	12.1	Org. Electron. 53 (2018) 191-197.
BPyPmIr	/	62.8	18.7	Mater. Chem. Front. 3 (2019) 376-384.

$(2\text{-Flfupy})_2Ir(acac)$	(0.57, 0.42)	21.8	9.1	Org. Electron. 53 (2018) 191-197.
$Ir(pyiq)_3$	/	22.51	8.71	Dyes and Pigments 185 (2021) 108880
$Ir(DPA\text{-}Flpy\text{-}CF_3)_2acac$	(0.64,0.36)	32.4	19.3	J. Mater. Chem. C. 4 (2016) 5787-5794.
$(PPQ)_2Ir(acac)$	(0.66, 0.34)	0.4	0.5	J. Mater. Chem. C. 5 (2017) 5749-5756.
$D\text{-}(PPQ)_2Ir(acac)$	(0.67, 0.33)	8.7	11.1	J. Mater. Chem. C. 5 (2017) 5749-5756.
D1	(0.66, 0.34)	39.8	24.7	This work
D2	(0.67, 0.33)	95.4	31.3	This work
D3	(0.41, 0.58)	17.2	12.3	This work

References

[1] G. Lu, R. Wu, N. Li, et al., J. Mater. Chem. C. 10 (2022) 17303-17308.